Comparative study on the influence of hydrodynamic conditions in the corrosion behavior of a 1018 carbon steel using a green inhibitor in brine-CO_2 solution

J. Henao,[1] A. Torres,[2] O. Sotelo-Mazon,[3,4]* S. Valdez-Rodriguez,[5] C. Poblano-Salas,[6] C. Cuevas-Arteaga,[4] J. Corona-Castuera,[6] J.J. Ramos-Hernandez[5] and M. Casales-Diaz[5]

[1]*CONACYT-CIATEQ A.C., Parque Industrial Bernardo Quintana, Av. Manantiales 23-A, 76246, Qro., México*
[2]*Tecnológico de Monterrey, Av. Carlos Lazo 100, Santa Fe, La Loma, 01389, Álvaro Obregón, CDMX, México*
[3]*Facultad de Ciencias Químicas e Ingeniería, UAEM, Av. Universidad 1001, 62209, Cuernavaca, Mor., México*
[4]*Centro de Investigación en Ingeniería y Ciencias Aplicadas, UAEM, Av. Universidad 1001, 62209, Cuernavaca, Mor., México*
[5]*Instituto de Ciencias Físicas, UNAM, Av. Universidad 1001, 62210, Cuernavaca, Mor., México*
[6]*CIATEQ A.C., Parque Industrial Bernardo Quintana, Av. Manantiales 23-A, 76246, Qro., México*
**E-mail: oscarsotelo.m@hotmail.com*

Abstract

The corrosion behavior of a 1018 carbon steel was studied by electrochemical techniques under hydrodynamic conditions employing *N*-hydroxyethylimidazoline derivatives of avocado oil as a green corrosion inhibitor. The corrosion behavior of the steel surface under hydrodynamic flow conditions before and after the addition of the green corrosion inhibitor was evaluated by means of the rotating cylinder method using rotation speeds of 0, 10, 100, 500, 1000, and 2000 RPM. The inhibitor concentration was set at 25 ppm (7.29×10^{-5} mol/L) in all conditions studied. The results display a high corrosion resistance of the carbon steel surface at a rotation speed of 1000 RPM in the absence of inhibitor, which is attributed to the formation of a protective $FeCO_3$ layer. When the inhibitor is added to the electrolyte, the highest corrosion resistance is observed for the samples evaluated under static conditions and the lowest rotational speeds. In the presence of the inhibitor, the carbon steel surface shows a decrease in the corrosion resistance as the rotation speed increases above 500 RPM. Interestingly, the addition of the inhibitor promotes a uniform corrosion process on the steel surface under zero rotation and low rotational speeds, and a localized corrosion process for high rotational speeds, respectively. The results suggest that dynamic conditions are associated to a change in the inhibitor concentration at the metal surface, which influences in a negative way the protective effect of the inhibitor.

Received: October 5, 2022. Published: December 29, 2022 doi: 10.17675/2305-6894-2023-12-1-1

Keywords: *green corrosion inhibitor, imidazoline, electrochemical techniques, hydrodynamic conditions, CO_2 corrosion.*

1. Introduction

Carbon steels have extensive applications due to their wide range of achievable mechanical properties. Industrial applications of carbon steels are mainly associated with the fabrication of tools, machinery parts, automobile parts and structural components including gears, blades, shafts, springs, dies, rails, and pipelines [1]. Some structural applications of carbon steels in the oil&gas transportation industry arise from their mechanical strength, weldability, and low cost. However, one disadvantage of these materials is their poor corrosion resistance in environments containing acidic and chloride solutions [2].

It is well known that corrosion of carbon steels is often promoted by the presence of CO_2 in the environment. For instance, when water and brine are exposed to CO_2, carbonic acid (H_2CO_3) is usually produced. This chemical reaction is often carried out within hydrocarbon pipelines where carbonic acid and NaCl are the main corrosive agents. Corrosion of carbon steels caused by CO_2 is known as "sweet corrosion" associated with either a pitting or uniform corrosion process [3]. The sweet corrosion process also promotes the formation of iron carbonate scale ($FeCO_3$) on the surface of the alloy; the scale formation depends on the pH of the solution, which should be between 4 and 6, and occurs at temperature values above 50°C. If the product of the local concentrations of iron (Fe^{2+}) and carbonate (CO_3^{2-}) ions exceed the solubility limit in the electrolyte, the formation of $FeCO_3$ is reached. This precipitate acts as a protective layer on the steel, reducing the corrosion rate [4, 5]. It is worth to mention that corrosion is not avoided by the precipitation of $FeCO_3$, since the formation of this scale is related to the presence free-scale active regions at the metal surface [6].

One common practice to mitigate corrosion in industrial petrochemical pipelines is the addition of corrosion inhibitors into the fluids. Corrosion inhibitors act by adsorption on the metal surface; this adsorption can be either physical or chemical depending on the chemical structure of the inhibitor, the state of the metal surface, and the type of corrosive medium [7, 8]. Organic compounds such as imidazoline, amides, amines, and their salts can act successfully as corrosion inhibitors [9], in particular when these are adsorbed on the metal surface forming a film that repels water molecules. A recent study suggest that organic corrosion inhibitors can also improve corrosion resistance of carbon steels by a double action, i.e. by adsorption on the metal surface and by simultaneously protecting the iron carbonate scales previously formed [10].

Nowadays, many efforts have been devoted to produce green corrosion inhibitors from oleic sources like coffee, rice, palm, castor, soy, or corn oils, which are used in the petroleum industry since these have shown good performance to mitigate corrosion in pipelines and

especially because they are non-toxic and synthetized from eco-friendly products. The performance of green inhibitors is a function of their chemical structure. For instance, the length of the hydrocarbon tail in the imidazoline structure (hydrophobic chain) can be extended during the synthesis process when oleic sources are used, promoting a change in the inhibition performance of the imidazoline compound at the metal surface [11]. Due to fact that the avocado fruit has high oil content (15–30%) which is unsaturated and the predominant fatty acid is oleic, a green corrosion inhibitor was synthetizing from waste avocado oil, which can lead to reduce the cost of inhibitor synthesis with respect to other synthesis strategies. Also, the fact that the inhibitor can be obtained from waste is important because it does not affect the avocado farming as a source of food for humans, being a good way of developing sustainable inhibitors.

Usually, laboratory characterization tests for the evaluation of green corrosion inhibitor performance are carried out under stagnant conditions. However, corrosion predictions based on stagnant tests are often inaccurate for real applications, mainly due to factors such as fluid movement [12]. For instance, when a fluid is under movement, mechanical shear stresses can occur on the metal surface, which can contribute to the detachment of corrosion products and modify the adsorption rate of the corrosion inhibitor [9]. Previous studies [13] have observed that carbon steel in CO_2-rich environments at subcritical flow intensities presents a limited formation of carbonate layers. Even in the presence of inhibitor, dynamic conditions can promote a phenomenon known as flow induced localized corrosion (FILC). This process initiates with cracks growing in the carbonate scale, which is followed by spalling and initiation of localized corrosion [13]. Previous studies also suggest that mechanical shear stresses produced under dynamic flow conditions can affect the corrosion resistance of the system, in particular due to the removal of the inhibitor films [6].

In order to evaluate the performance of corrosion inhibitors under flow dynamic conditions, a rotating cylinder electrode equipment can be used; this assembly has the advantage to provide information about the influence of turbulent flow on the corrosion rate of metallic alloys in corrosive environments [9]. Previous studies have reported that corrosion performance of carbon steel can be evaluated by means of a rotation assembly test [14]. The test results can be compared against the corrosion performance of the steel observed in common situations such as in straight pipe flows [14]. Fortunately, this type of approaches allows to accurately simulate, in the laboratory, real transportation conditions of oil and gas through steel pipelines.

The aim of this work is to study the effect of dynamic flow conditions on the corrosion performance of a 1018 carbon steel alloy by using *N*-hydroxyethylimidazoline derivatives of avocado oil as a green corrosion inhibitor. Specifically, this work is focused to study the effect of the presence/absence of a green corrosion inhibitor in a corrosive environment on the corrosion behavior of the steel surface. Changes in the corrosion rate of the steel surface promoted by the variation of the dynamic flow conditions induced by rotating the sample

were evaluated. This study seeks to reveal how hydroxyethylimidazoline derivatives of avocado oil act as a corrosion inhibitor under simulated flow pipeline conditions.

2. Experimental procedure

2.1. Material

A commercial 1018 carbon steel rod was used as testing material (working electrode) in the present study. The composition of this material is reported elsewhere as 0.15–0.20% C, 0.60–0.90% Mn, 0.040% P, 0.050% S, and Fe balance [15]. The working electrodes were machined into 12 mm diameter and 8 mm thickness cylindrical coupons. Before each test, the cylinders were ground employing SiC emery paper down to P 600 grade, then cleaned with acetone and distilled water.

2.2. Test solution and cell arrangement

N-Hydroxyethylimidazoline derivatives of avocado oil were employed as a corrosion inhibitor. The synthesis of this inhibitor was reported in a previous study [10]. The inhibitor concentration employed in all the experiments was stablished at 25 ppm (7.29×10^{-5} mol/L) based on an optimal inhibitor concentration reported in a previous work [16]. The corrosive medium consisted of 3% NaCl (wt.%) and diesel in a 90/10 proportion in volume percentage, respectively.

The rotation test assembly consisted of a glass cell with three electrodes and a total electrolyte volume of 400 ml. A graphite rod and a platinum plate were used as counter and reference electrodes, respectively. To promote hydrodynamic flow conditions, the working electrode was mounted on a Model 636 EG&G Princeton Applied Research Ring Electrode System. Rotation speeds of 10, 100, 500, 1000, and 2000 RPM were applied to the working electrode. Initially, the system was de-aerated by bubbling CO_2 for 1 h at 70°C. Thereafter, the working electrode was immersed into the electrolyte and 1 hour later the corrosion inhibitor was added.

2.3. Electrochemical measurements

Potentiodynamic polarization curves (PC), linear polarization resistance (LPR), and electrochemical impedance spectroscopy (EIS) were performed to evaluate the corrosion inhibitor performance under static and dynamic conditions (rotation speeds of 0, 10, 100, 500, 1000, and 2000 RPM). The electrochemical measurements were carried out employing a Gamry Interface 1000 Potentiostat/Galvanostat. PC test was conducted at a sweep rate of 1 mV/s and at a scanning range from –400 to 800 mV with respect to the corrosion potential (E_{corr}). LPR test was performed applying an overpotential of ±10mV with respect to E_{corr} at a sweep rate of 1 mV/s. EIS measurements were carried out applying a perturbation amplitude of 10 mV, in a frequency range of 100,000–0.01 Hz. LPR and EIS measurements were conducted for 24 h.

The parameters calculated from the electrochemical dynamic test were the fluid velocity (*V*), Reynold number (*Re*) and electrode wall shear stress (τ). These parameters are relevant to understand how the physical interaction between the fluid and the surface can affect the corrosion rate of the alloy [12]. The flow velocity "*V*" [m/s] was obtained according to the following equation:

$$V = w(r) \tag{1}$$

where "*r*" is the electrode radius (0.00635 m) and "*w*" is the angular velocity (RPM); the conversion factor from RPM to rad/s units is given by $w = x$ rev/min (2π rad/60 s).

The Reynolds number (Re), which is the ratio between the viscous to inertial forces, was obtained by using the following equation:

$$Re = \frac{Vd}{\upsilon} \tag{2}$$

where "*d*" is the electrode diameter (0.0127 m) and "υ" is the kinematic viscosity, which in turn was calculated as $\upsilon = \mu/\rho$ [9]. The fluid density "ρ*"* value used in this work was 1086.75 kg/m^3 whereas the dynamic viscosity "μ*"* value was ~0.0034 Pa·s, which was calculated using a viscometer (Brookfield). The Re number is often used to categorize fluid systems in which the effect of viscosity is important in controlling the fluid flow pattern, that is, to determine when laminar or turbulent flow can occur.

The shear stress at the wall (τ), understood as the forces acting on the fluid by the movement imposed to the electrode surface, was calculated according to the following equation [12, 17]:

$$\tau = 0.0791\ Re^{-0.3} \cdot \rho \cdot w^2 \cdot r^2 \tag{3}$$

The shear stress in the electrode wall is an important parameter related to the hydrodynamic flow conditions that can influence the corrosion rate of the system. Variations of this parameter can either promote delamination of the corrosion products or desorption of the inhibitor from the metal surface [18]. Finally, SEM analysis was carried out using a JEOL JSM IT500 electron microscope to analyze the degradation of the samples surface at the end of the tests.

3. Results and Discussion

3.1. Flow parameters

It is well known that flow conditions within pipelines can be recreated by using a rotating cylinder. Particularly, when experimental conditions involve transition from laminar to turbulent flow [19]. Recent studies have carried out experiments under dynamic flow conditions to determine the effect of laminar and turbulent regimes on the corrosion process of carbon steel alloys [18]. Laminar flow conditions are defined when the fluid molecules follow smooth paths within a liquid layer, with each liquid layer also moving smoothly with

respect to each other; that is, no-mixing conditions are assumed to occur. On the other hand, turbulent flow involves disruption among liquid layers and promotes liquid mixing and changes in liquid pressure and velocity [9]. The onset of turbulent fluid conditions can usually be predicted by the Reynolds number (*Re*), which is the ratio between the kinetic energy and viscous damping of the fluid. Depending on the configuration of the pipeline, different types of regime flow can occur. For instance, when a liquid is transported through a pipeline and shows a Re value of ~2000, it is an indication of a transitional regime from laminar to turbulent flow. When the *Re* values are around ~100,000, the fluid achieves full turbulence flow [20, 21, 12]. On the other hand, when experiments are carried out in a rotating cylinder system to simulate flow conditions within a pipeline, the transition from laminar to turbulent flow can also be observed, but the *Re* values are often lower than those calculated for the same flow regime within a pipeline; that is, when the same liquid is studied in a rotating cylinder electrode, the transition from laminar to turbulent flow is predicted for *Re* values of ~200 [21, 22, 23].

In the present study, *Re* values were calculated for the different experimental conditions studied. For instance, according to Table 1, for the CO_2-saturated 3% NaCl–diesel solution laminar flow was promoted when the rotational speed was set at 10 RPM, while turbulent flow was obtained for rotational speed above 100 RPM.

Table 1. Re and τ calculated for the samples evaluated under CO_2-saturated 3% NaCl-diesel solution.

Sample rotational speeds (RPM)	V (m/s)	Re	τ (Pa)
0	0	0	0
10	0.006	27	0.001
100	0.066	270	0.070
500	0.332	1350	1.100
1000	0.664	2700	3.552
2000	1.329	5400	11.542

3.2 Polarization Curves

The potentiodynamic polarization curves for the carbon steel samples evaluated without inhibitor are presented in Figure 1. The results reveal that the noblest potential value was obtained for zero rotation, while the most active potential values were obtained under hydrodynamics flow conditions. This behavior is mainly related to the oil phase (diesel) in the corrosive solution, which can behave like a cathodic type inhibitor [24]. In fact, Faysal Fayez Eliyan *et al.* [25] studied the corrosion behavior of a API-X100 steel in a solution containing an oil phase (diesel). The authors reported a reduction in the corrosion rate and

lower corrosion potential values due to the presence of diesel in the electrolyte, in particular for a diesel content of 10 % in volume.

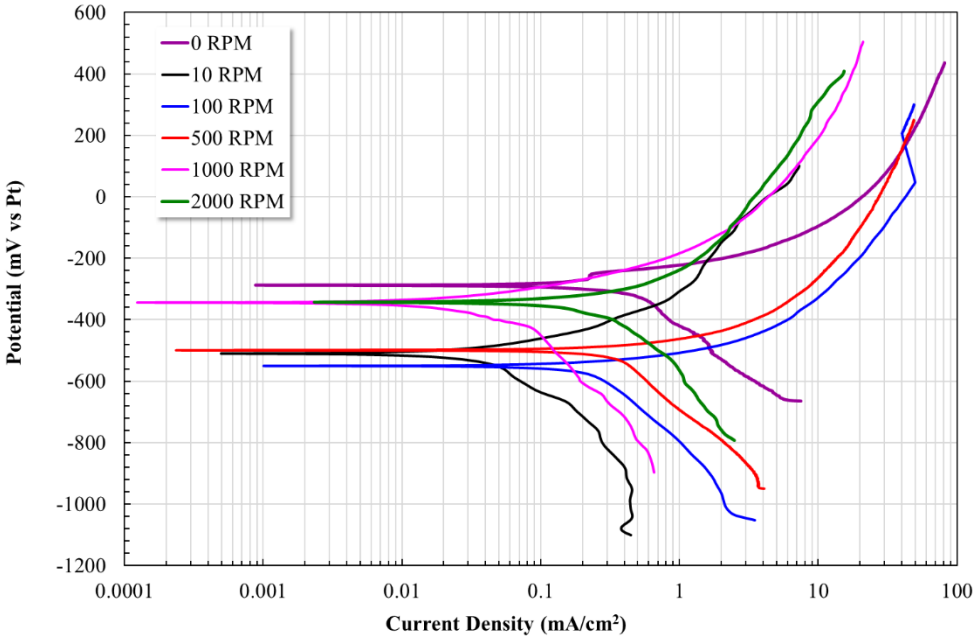

Figure 1. Polarization curves of a 1018 carbon steel in 3%NaCl–diesel solution with bubbling CO_2 for different rotational speeds (0, 10, 100, 500, 1000, and 2000 RPM) at 70°C, in the absence of inhibitor.

As can be seen in Figure 1, all the anodic branches displayed an active behavior. The potentiodynamic curves showed an increment in the current density when the potential become more anodic, which is associated with metal dissolution due to the instability of species adsorbed at the metal surface, becoming unstable at high polarization potentials. This fact suggests that adsorbed species leave the metal surface quickly as the anodic metal dissolution occurs; moreover, some authors suggest that rotational speed can also be an important factor for increasing the species desorption from the steel surface [7, 26]. In addition, the behavior of the anodic current branch obtained in this study is similar in all samples, regardless of the rotational speed employed. M.E. Olvera-Martinez *et al.* concluded that a charge transfer phenomenon is carried out in the anodic reaction when the temperature of the system is constant [9]. The results obtained by M.E. Olvera-Martinez *et al.* are then in agreement with the results reported in the present study. From Table 2, the B_c values increased by increasing the rotational speed. This fact suggests that cathodic curves are more remarkably controlled by mass transport as the rotational speed increases [27]. In this sense, the cathodic process is flow dependent and is associated with the diffusion of H^+ ions from the bulk solution towards the steel surface [9]. The reduction reactions happening in the process can be attributed to the reaction of H_2CO_3 into HCO_3^-, since it is favored for pH

values from 4 to 6 [28, 29]. A measured pH value of 6 was obtained in the present work as also reported in a previous study [30].

The corrosion current density values (i_{corr}) were very similar among all the samples, although samples evaluated at 10 and 1000 RPM did not follow this trend. The i_{corr} values obtained for both samples suggested a slow corrosion process arising from the surface conditions promoted by the flux experienced at these rotational speeds, as will be further discussed.

Table 2. Electrochemical parameters from polarization curves obtained for different rotational speeds at 70°C in the absence of inhibitor.

Sample rotational speeds (RPM)	E_{corr} (mV *vs.* Pt)	i_{corr} (mA/cm^2)	B_a (mV/decade)	B_c (mV/decade)
0	–287	0.485	155	368
10	–510	0.0661	148.5	460.1
100	–550	0.307	87	493.7
500	–500	0.451	99.1	537.2
1000	–343	0.0531	118.9	751.6
2000	–342	0.488	204.7	723.4

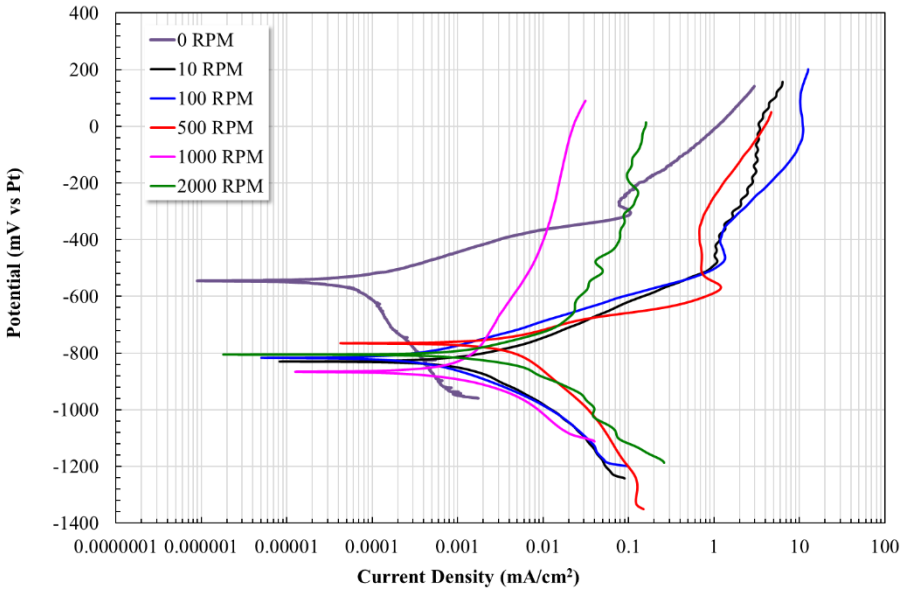

Figure 2. Polarization curves of a 1018 carbon steel in a 3%NaCl–diesel solution with bubbling CO_2 for different rotational speeds (0, 10, 100, 500, 1000, and 2000 RPM) at 70°C, in the presence of inhibitor (7.29×10^{-5} mol/L).

Figure 2 shows the potentiodynamic polarization curves for the 1018 steel samples evaluated in the presence of the corrosion inhibitor. The noblest potential value was –545 mV, which was obtained for the sample evaluated at 0 RPM. When the rotational speeds were increased, the potential values observed in the samples were between –766 and –866 mV. Interestingly, the potential values of the samples evaluated in the presence of the inhibitor had more active values with respect to the samples evaluated without inhibitor. This fact can be associated with the adsorption of both inhibitor and diesel on the metal surface, behaving as cathodic-type inhibitors [16, 25]. This phenomenon contributes to suppress the cathodic reactions in the system due to the adsorption of the inhibitor at the cathodic sites [31]. The cathodic reactions in the CO_2-saturated aqueous system can be summarized as follows [32]:

$$2H_2CO_3(aq) + 2e^- \rightarrow H_2(g) + 2\,HCO_3^-\,(aq) \quad (4)$$

$$2H^+(aq) + 2e^- \rightarrow H_2(g) \quad (5)$$

$$2H_2O(l) + 2e^- \rightarrow H_2(g) + 2OH^-(aq) \quad (6)$$

Table 3 presents the electrochemical parameters obtained for the samples evaluated in the presence of the green corrosion inhibitor in the solution. The results show the lowest i_{corr} value for the sample evaluated at 0 RPM. However, under hydrodynamic flow conditions, the i_{corr} values increased about two orders of magnitude with respect to the values displayed for static flow conditions; this behavior is associated with an increment of the rotating rate affecting the adsorption of the inhibitor, leaving the steel surface exposed to the electrolyte [26]. Overall, the i_{corr} values were lower in the samples evaluated with inhibitor in comparison with the inhibitor-free counterparts. This fact can be associated with the enhanced corrosion resistance of the system due to the presence of the inhibitor at the metal surface. In addition, the anodic branches showed a similar behavior for the different rotational speeds. Therefore, above the corrosion potential, E_{corr}, the results displayed an increment in the current density, followed by a decrement in the anodic branch slopes where a notorious tendency to passivate to all rotating rate was observed, mainly at low rotational speeds. This fact suggests a slowdown in the anodic reaction, which is related to the dissolution of Fe ($Fe \rightarrow Fe^{2+} + 2e^-$), resulting in the formation of a more protective layer on the steel surface [11].

Table 3. Electrochemical parameters from polarization curves obtained for different rotational speeds at 70°C, in the presence of inhibitor.

Sample rotational speeds (RPM)	***E*corr (mV *vs*. Pt)**	***i*corr (mA/cm²)**	***Ba*** **(mV/decade)**	***Bc*** **(mV/decade)**
0	–545	0.000074	87	385
10	–830	0.00217	125.2	248.4

Sample rotational speeds (RPM)	E_{corr} (mV *vs.* Pt)	i_{corr} (mA/cm^2)	*Ba* (mV/decade)	*Bc* (mV/decade)
100	–818	0.00052	97.1	149.5
500	–766	0.00461	83.8	313.6
1000	–865	0.00176	626.6	182.7
2000	–805	0.00776	398.2	279.6

3.3. Linear Polarization Resistance (LPR)

The evolution of the polarization resistance of 1018 carbon steel in the absence of inhibitor is shown in Figure 3. The polarization resistance (R_p) values are a function of the electrode rotational speeds. For instance, the sample evaluated under static flow conditions presented the lowest R_p value, but when rotational movement was applied to the electrode, providing kinetic energy to the fluid, then an increment in the R_p values was observed. Interestingly, the increment in the R_p values was not directly proportional to the rotational speed of the electrode, suggesting the involvement of other variables in the corrosion process, as will be further discussed. The sample evaluated at a rotational speed of 10 RPM showed a R_p value of 714.8 Ohm·cm^2 at the end of the test; when the rotational speed was increased to 100 and 500 RPM, the R_p values were superior to that obtained under static conditions (59.13 Ohm·cm^2) and lower than that of the sample evaluated at 10 RPM. The R_p values for the samples evaluated at 100 RPM and 500 RPM were 279.5 and 90.6 Ohm·cm^2, respectively. When the samples were evaluated at 1000 RPM, the experiments displayed an increment in the R_p value (1528 Ohm·cm^2) with respect to that of the sample evaluated at 10 RPM. Finally, when the rotational speed was 2000 RPM, a decrease in the R_p value (130.4 Ohm·cm^2) was observed again with respect to that of the sample evaluated at 10 RPM. This random behavior has been previously reported in the literature for NaCl and CO_2-saturated NaCl solutions [9, 27, 33] and can be attributed to the presence of a protective layer and diesel adsorption on the steel surface. Particularly, previous studies suggest the formation of a $FeCO_3$ layer on the steel surface that blocks active sites at the surface and restricts the transport of active species [34]. It is important to point out that the effectiveness of the $FeCO_3$ layer as a protective barrier depends on temperature, CO_2 partial pressure, and pH values. For example, below 150°C the formation of $FeCO_3$ precipitates as an exclusive corrosion product occurs, forming a protective layer. This layer leads to a decrease in the corrosion rate, in particular when the temperature of the system exceeds 60°C. The formation of a dense $FeCO_3$ layer has an enhanced protective function when the temperature of the system is above 90°C [35].

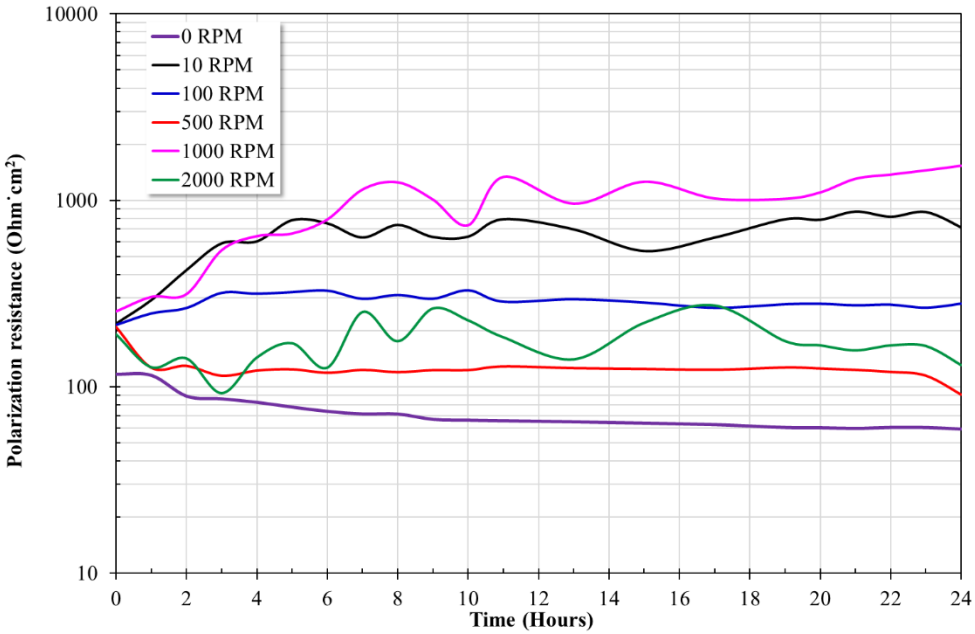

Figure 3. LPR plot of a 1018 carbon steel at 70°C in 3%NaCl–Diesel solution with CO_2 bubbling at different rotational speeds (0, 10, 100, 500, 1000 and 2000 RPM) in the absence of inhibitor.

The lowest R_p value (59.13 Ohm·cm^2) obtained in the present study under standstill conditions can be associated with the reaction of Fe ions with carbonic acid species and bicarbonate ions, leading to the formation of a $FeCO_3$ layer with poor protective performance. Interestingly, Hua *et al.* reported experiments performed at 90°C, obtaining a dense $FeCO_3$ layer. Such $FeCO_3$ layer promoted a decrease in the corrosion rate of X65 carbon steel evaluated in brine solution [35]. Due to the lower temperature (70°C) employed in the present study with respect to that reported by Hua *et al*., this carbonate layer may be heterogeneous, including some morphological defects such as pores and cracks (see Section 3.4), which could not stop the corrosion process associated with the interaction of the electrolyte and the metal surface [7, 16].

Regarding the comparative between static and dynamic conditions (Figure 3), the results show an increment in the corrosion resistance values under hydrodynamic conditions that can be attributed to the movement of the fluid. Dynamic conditions allow the mass transport of species (H_2CO_3 or HCO_3^-) from the bulk solution to the steel surface, promoting a faster precipitation of $FeCO_3$, as it happened from 10 RPM. In fact, the fluid movement can also contribute to increase the concentration of diesel at the metal surface. Both $FeCO_3$ layer and adsorbed diesel may contribute to increase the corrosion resistance of the samples under dynamic conditions. Previous studies [30, 36] suggest some mechanisms associated with the presence of diesel in the electrolyte. Firstly, oil phase can be adsorbed on the metal surface reducing the corrosion rate due to the reduction in the mass transfer process. Secondly, an

oil-water emulsion can be formed, allowing the oil to diffuse through the aqueous phase and reach the steel surface. This fact can limit the diffusion of aggressive species towards the metal surface. Thirdly, a multiphase fluid, involving CO_2 gas, oil and water, can be formed, presenting a solubility of diesel around 0.5–7 mg/L in water at room temperature. This multiphase fluid can favor the formation of water-soluble fractions, containing a mixture of C4 to C6 nonaromatic hydrocarbons. Then, these water-soluble fractions can be adsorbed on the steel surface, reducing its corrosion rate by limiting the mass transport of aggressive species towards the metal surface [30, 36].

Unlike the sample evaluated at 10 RPM, the R_p values obtained at 100 and 500 RPM decreased as testing time progressed, which is related to the occurrence of fluid wall shear stresses at the electrode surface. It has been reported that fluid wall shear stresses $\leq$0.2 Pa affect the formation of the $FeCO_3$ layer in absence of inhibitor evaluated both in NaCl and NaCl–CO_2 solutions, starting a process of localized corrosion (see Table 1) [13, 37]. Otherwise, the samples evaluated at 1000 RPM displayed an increase in corrosion resistance, which is related to the stronger movement of the fluid, allowing the diesel to reach the metal surface more easily. As a result, the oily part soluble in the NaCl solution could act as inhibitor, which along with the $FeCO_3$ layer, may provide protection to the metal surface, limiting the mass-transfer of aggressive species [26, 38]. On the other hand, at 2000 RPM, the R_p value decreases, which can be related to remotion of the $FeCO_3$ layer and/or the desorption of diesel due to mechanical forces (τ) caused by the solution high kinetic energy [9]. Therefore, we can assume that the fluid kinetic energy shows different behavior in a multi-phase solution. By one hand, for certain rotational speeds the movement of the fluid helps to enhance the diesel adsorption and mass transfer of bulk solution to the metal surface to improve the formation of the $FeCO_3$ layer. On the other hand, if the fluid movement is not highly enough to promote the formation of a protective $FeCO_3$ layer, the wall shear stress of electrode can initiate a process of localized corrosion and the adsorption and desorption of diesel by mechanical effects [18].

The polarization resistance of the 1018 carbon steel alloy in presence of inhibitor for different rotation speeds is presented in Figure 4. During the first hours, an increment of corrosion resistance is observed for all conditions, except at 2000 RPM. The enhanced corrosion resistance in these samples is associated with a better adsorption process of the inhibitor on the metal surface with short pre-corrosion time (approximately 2 h), that is, freshly ground specimens [26, 39, 40]. After 24 h testing, the highest corrosion resistance (R_p) was obtained in the present study under stagnant conditions (0 RPM), while the lowest R_p value was obtained at the highest rotation speed (2000 RPM). It is worth mentioning that samples evaluated with inhibitor presented the best corrosion resistance if compared against those evaluated without inhibitor, regardless of the rotational speeds employed (Figures 3 and 4).

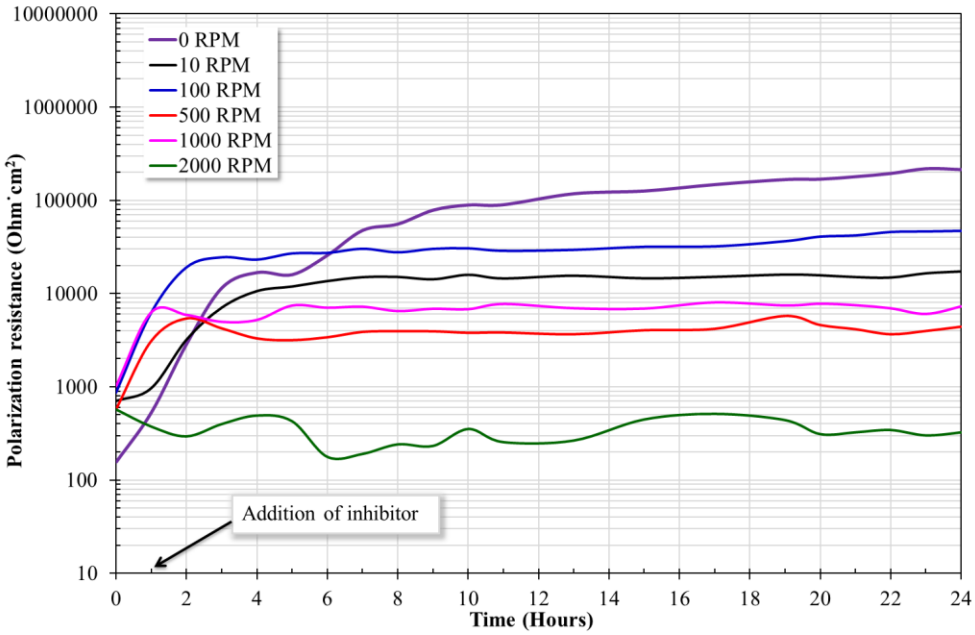

Figure 4. LPR plot of a 1018 carbon steel at 70°C in 3%NaCl–Diesel with CO_2 bubbling at different rotational speeds (0, 10, 100, 500, 1000 and 2000 RPM) in the presence of inhibitor.

It is well-known that the corrosion inhibition process of organic inhibitors is firstly carried out by adsorption on the metal surface, promoting the desorption of water molecules. Then, the inhibitor interacts with Fe^{2+} ions ($Fe \rightarrow Fe^{2+} + 2e^{-}$), which are generated by metal dissolution leading to form metal–inhibitor complex species $[Fe–Inh]^{2+}$ [22]. Nevertheless, under hydrodynamic conditions, the inhibitor may show a different performance; for instance, fluid flow increases mass transport of inhibitor molecules, which in turn promotes a higher concentration of such molecules on the metal surface resulting in an increased inhibition performance. In the present study, the inhibitor performance increased when the rotational speed was set at 100 RPM. Conversely, it has also been mentioned that a high flow velocity promotes mass transport of Fe^{2+} ions away from the metal surface to the bulk solution, decreasing the concentration of $[Fe–Inh]^{2+}$ complex species on the electrode surface, resulting in a negative effect on the protection at the surface [41]. Furthermore, it has been found that when the rotational speed was set above 100 RPM the shear stress on the electrode surface wall leads to the desorption of either the inhibitor layer or $[Fe–Inh]^{2+}$ complex species, causing a decrease of the corrosion resistance [22], as it was observed in the present study.

Table 4 shows the inhibition efficiency percentage (%IE) values obtained from the LPR measurements estimated from equation (7). The results display a %IE value of 99.97% for the samples evaluated under static conditions; however, this efficiency was affected when the experiments were carried out under dynamic conditions. The highest drop in the %IE values was obtained for the samples evaluated at 1000 and 2000 RPM rotational speeds, with %IE values of 79.04 and 59.62 %, respectively. These results are attributed to the flow

of the electrolyte over the metal surface that can produce a decreased %IE by the reduction of the inhibitor concentration per unit surface. Some studies have also suggested that permeation of the electrolyte through the protective film is favored by the shear stresses at the metal surface, which promoted the reduction in the inhibitor efficiency [40, 42, 43]. Despite the reduction in the inhibitor efficiency under dynamic conditions, Table 4 shows that RPL values are always higher for the inhibited solution than those for the inhibitor-free counterpart, which confirms that the corrosion resistance of the steel samples increases by adding the inhibitor even under dynamic conditions. Hence, optimal inhibitory conditions are achieved either under static conditions or by setting very low rotational speeds in order to allow the inhibitor molecules to interact with the metal surface.

$$\%IE = \left(\frac{RPL_{\text{inhibitor}} - RPL_{\text{blank}}}{RPL_{\text{inhibitor}}} \right) \cdot 100 \quad (7)$$

Table 4. %*IE* obtained from corrosion resistances values of RPL tests at various rotation speeds.

Sample rotational speeds (RPM)	**RPL-uninhibited solution (Ohm˙cm^2)**	**RPL-inhibited solution (Ohm˙cm^2)**	**%*IE***
0	59.13	213800	99.97
10	714.8	15210	95.30
100	279.50	46980	99.40
500	90.64	4386	97.99
1000	1528	7291	79.04
2000	130.4	323	59.62

3.4. Electrochemical impedance spectroscopy (EIS)

Figure 5 shows the EIS plots for the steel samples evaluated in the absence of inhibitor. The Nyquist plot (Fig. 5A) shows the formation of one capacitive semicircle for all conditions. The formation of these semi-circles indicates the occurrence of a corrosion process controlled by charge transfer, which, as discussed previously, confirms the contribution of the ohmic resistance associated with the corrosion products layer, *i.e.* $FeCO_3$. The results agree with RPL values obtained in section 3.3 for all the samples, displaying the highest semicircle diameters for the samples evaluated at 10 RPM and 1000 RPM. Interestingly, the results also show the formation of inductive loops at low frequency (inset in Fig. 5A), except for the sample evaluated at 1000 RPM. Previous studies associate the formation of an inductive loop to the relaxation process obtained by the adsorption of species on the metal surface, such as Cl^-_{ads} and H^+_{ads} and/or by the adsorption of intermediate products ($FeOH_{ad}$) formed during the dissolution of the base metal, stablishing a barrier to current flow [24, 44].

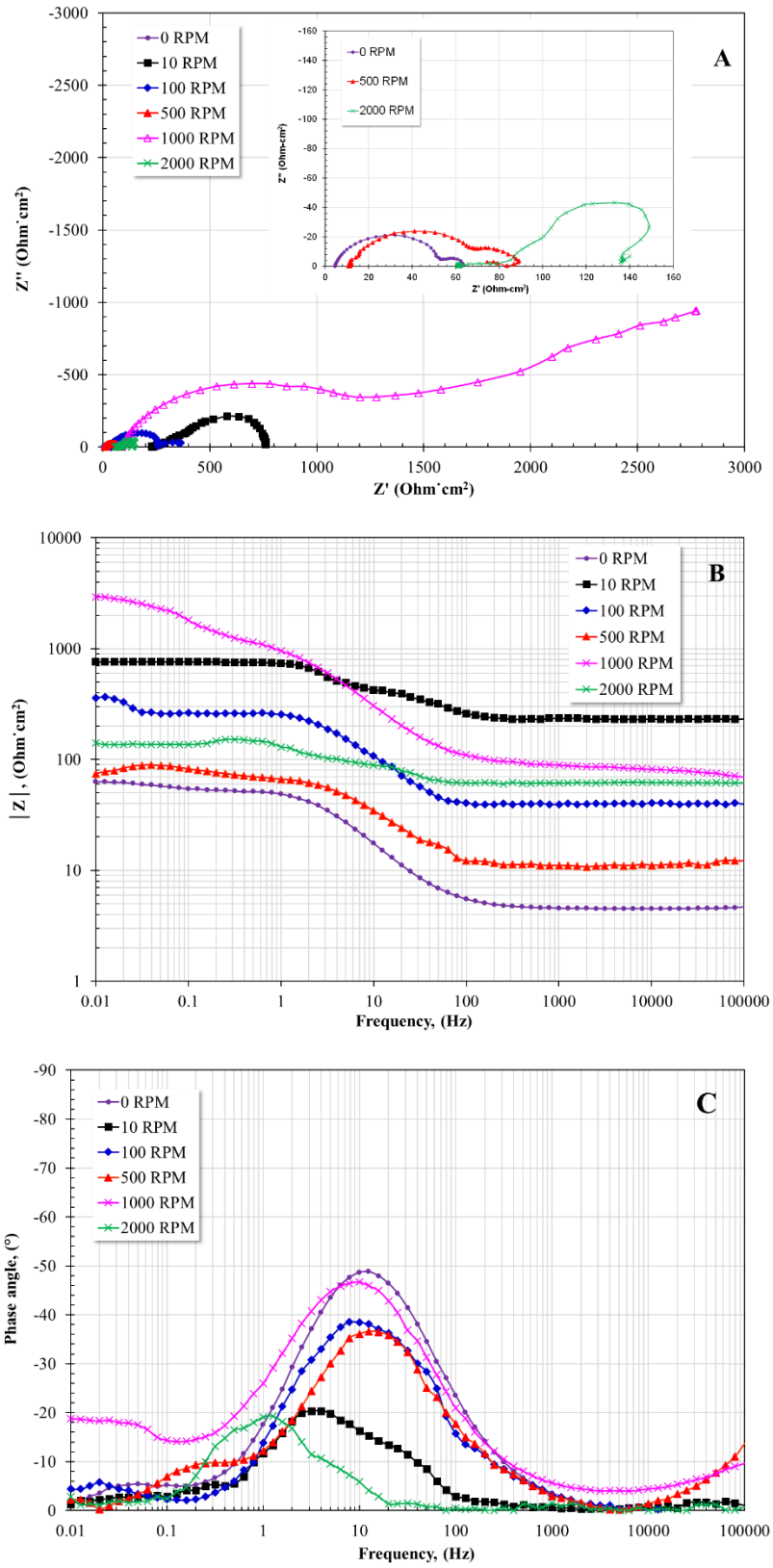

Figure 5. EIS curves of 1018 carbon steel at 70°C in 3%NaCl–Diesel with bubbling CO_2 for different rotational speeds (0, 10, 100, 500, 1000 and 2000 RPM) in the absence of inhibitor.

As deduced from the Nyquist plot (Figure 5B), the impedance module ($|Z''|$) also reveals that the lowest charge transfer resistance (R_{ct}) was obtained for the sample evaluated at 0 RPM, while the sample tested at 1000 RPM displayed the highest R_{ct}. In fact, the results show that the charge transfer resistance increases as soon as the electrode starts rotating and promoting fluid movement. This fact indicates that the adsorption process of species on the metal surface is improved by fluid motion. This result agrees with those in previous sections, which associate the enhanced corrosion resistance to the improved mechanisms of diesel adsorption at the metal surface as the rotational speed is increased. As suggested in previous studies [21, 45], the fact that at 1000 RPM the highest R_{ct} value was achieved can be associated with an increment in the mass transfer of both diesel and H_2CO_3/HCO_3^- species from the bulk solution to the metal surface. This contribution can be observed in Figure 5A, from the linear behavior observed at the end of the semi-circle in the sample evaluated at 1000 RPM. In this sense, the formation of the $FeCO_3$ layer and the role of diesel as inhibitor are both favored, leading to an increase in the corrosion resistance. Overall, there is not a constant increment in the charge transfer resistance of the samples as a function of rotational speed; instead, a random behavior was observed, which can be likely attributed to competing processes between the adsorption of diesel species and formation of the $FeCO_3$ protective layer [25].

On the other hand, the phase angle plot in Figure 5C presents the formation of a time constant for each rotational speed evaluated in this study. Samples tested at 0 RPM and 1000 RPM presented the highest phase angle values, close to 50 degrees. It is worth mentioning that, if the angle phase value is close to 90° the material follows a capacitive behavior, which is associated with the presence of a protective layer. If the phase angle lies around 50°, a corrosion process of mixed control (diffusion and charge transfer) can occur [30]. Conversely, samples evaluated at 10 RPM and 2000 RPM showed the lowest phase angle values, *i.e.* around 20 degrees. The low phase angles and the displacement of their peak values towards low frequency regions found for these samples can be associated with the presence of thin corrosion product layers at the metal surface. This fact agrees with similar phenomena reported in previous studies [10, 46], and can be attributed in the present work to the effect of shear stress and mass transport of H_2CO_3 or HCO_3^- towards the electrode wall. In particular, some authors reported that shear stress values between 7.7 and 15.4 Pa can disturb and decrease the efficiency of the protective film [40], as observed at 2000 RPM in this work.

Figure 6 shows EIS plots for the samples evaluated in the presence of inhibitor. Nyquist plot in Figure 6A shows the formation of semicircles in all conditions, indicating that the corrosion process was mainly conducted under charge transfer. Overall, Figure 6A displays a decrease in the semicircles diameter as the rotational speed is increased, indicating a decrease in the charge transfer resistance in comparison to the sample evaluated at 0 RPM. The standstill condition displays a straight line located at low frequencies, suggesting that the corrosion process is controlled by diffusion [16].

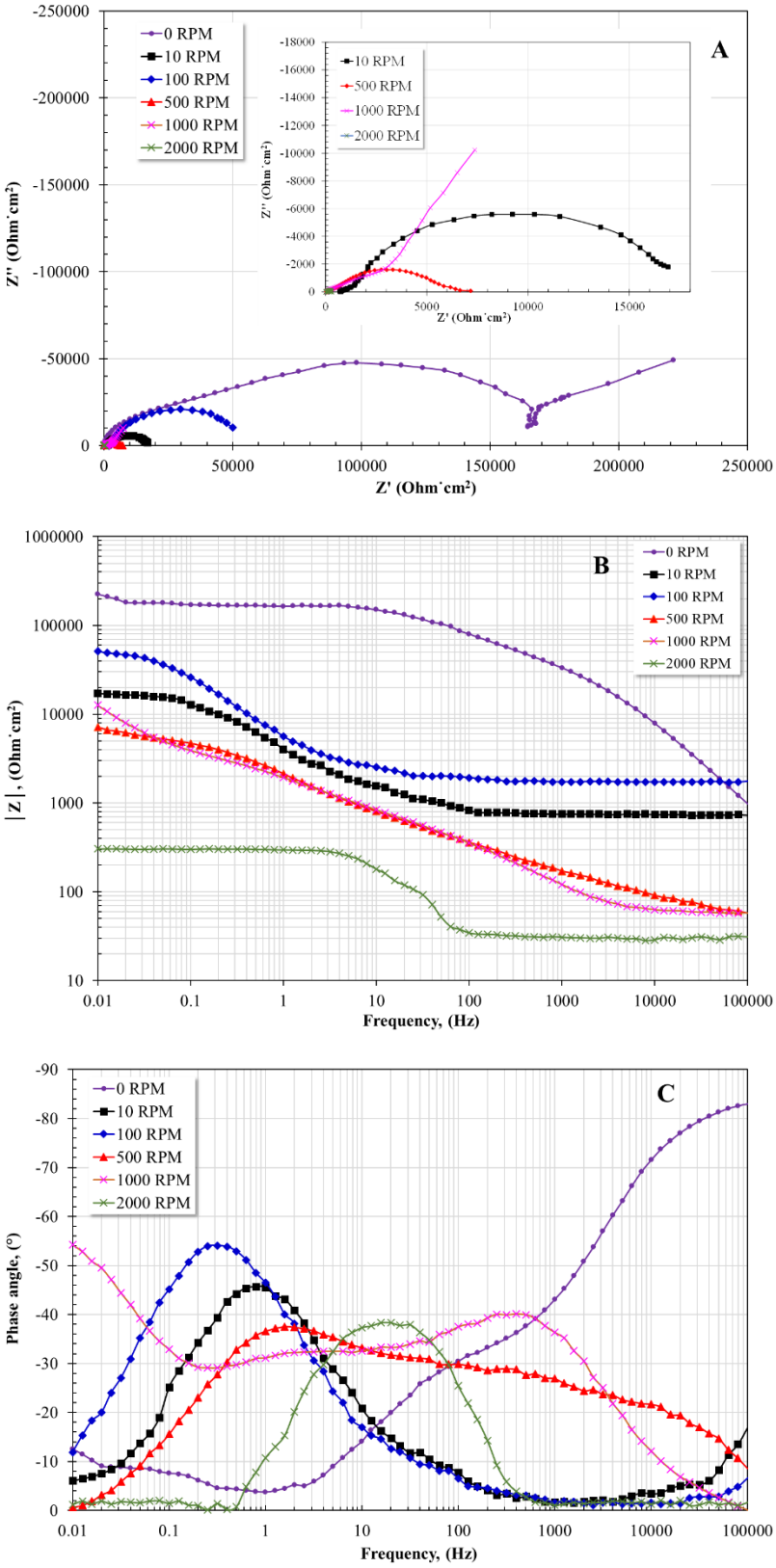

Figure 6. EIS curves of a 1018 carbon steel at 70°C in 3%NaCl-Diesel with bubbling CO_2 for different rotational speeds (0, 10, 100, 500, 1000 and 2000 RPM) in the presence of inhibitor.

Figure 6B presents the results of the impedance module plot of the samples evaluated with inhibitor. The |*Z*| module plot displays that the sample evaluated at 0 RPM had the highest charge transfer resistance (R_{ct}) followed by those evaluated at 10 RPM and 100 RPM, with values of 226636, 17003 and 51076 Ohm·cm^2, respectively. Moreover, the lowest corrosion resistance was obtained for the samples evaluated at 2000 RPM, which also confirms the results obtained in the RPL experiments previously discussed.

Interestingly, the phase angle plot in Figure 6C shows the formation of a time constant in all samples but for 500 and 1000 RPM conditions. Both conditions showed the formation of two and three time constants, respectively. When comparing these samples against the 0 RPM counterpart, the later display a high phase angle at high frequencies, which is associated with a capacitive behavior due to the presence of the inhibitor at the metal surface. However, fluid motion disturbs the adsorption of the inhibitor at the metal surface, causing the displacement of the time constants towards lower frequencies, as observed for the samples evaluated at 10 and 100 RPM. In addition, when the rotational speed is set at 500 and 1000 RPM, both high and low frequency time constants appear, which can be associated with the occurrence of inhibitor adsorption and disruption of the corrosion layer due to the increased shear stress experienced at the metal surface [47, 48, 49].

Usually, when the experiments are carried out in the presence of an inhibitor, the phase angle plot often displays two time constants [5, 7]. However, the results obtained for the samples evaluated at 10 and 100 RPM shows only a single time constant. It is then inferred that the values of R_{ct} are the sum of the contribution of both the electric double layer in the metal/corrosion products and the inhibitor film [50]. This behavior agrees with a study carried out by Shamsa *et al.* [51, 52] using an imidazoline-based corrosion inhibitor. The authors concluded that corrosion protection may be a function of two factors, the adsorption of inhibitor at the metal surface leading to the formation of a film and the presence of corrosion products. Since, they observed that in the presence of both an inhibitor film and $FeCO_3$ layer on the steel surface, the overall protection provided by the corrosion inhibitor was only of 25%.

Based on these results, the samples evaluated here at 10 and 100 RPM may show a closer behavior with respect to the sample evaluated under static conditions, originated from a most stable behavior of both the inhibitor film and the $FeCO_3$ layer. As mentioned previously, the shear stress values increased two and three orders of magnitude above 100 RPM, which could disturb the protective effect of these layers. Finally, when the rotational speed was set at 2000 RPM, most of the metal surface protection was provided by the $FeCO_3$ layer and its ability to support formation and re-dissolution, mainly caused by the high shear stress at the metal surface not allowing the complete establishment of the inhibitor film [51, 52].

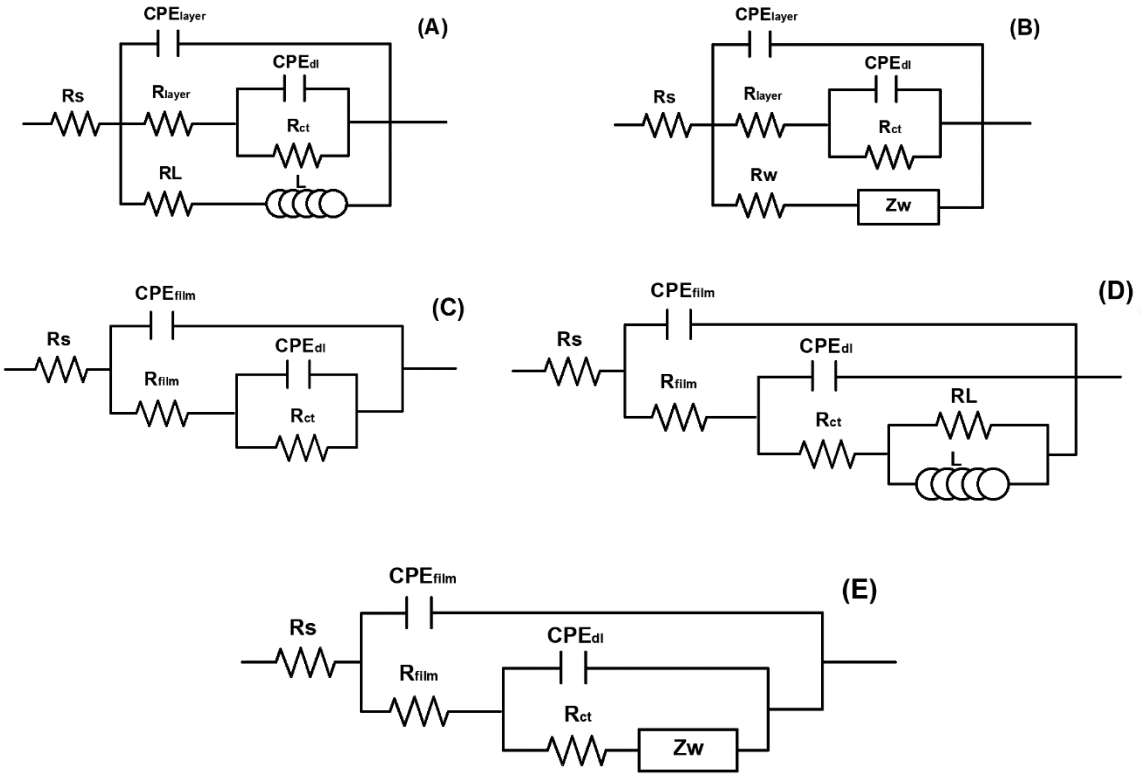

Figure 7. Electric circuits models used to simulate the EIS data for the samples evaluated under: (A) inhibitor-free solution at 10, 100, 500, and 2000 RPM, (B) inhibitor-free solution at 1000 RPM, (C) inhibited solution at 10 and 100 RPM, (D) inhibited solution at 500 and 2000 RPM, and (E) inhibited solution at 1000 RPM.

Figure 7 shows the electric circuits models used to interpret the EIS data in the absence and presence of inhibitor. The equivalent circuit model shown in Figure 7A was obtained for the samples evaluated at 10, 100, 500, and 2000 RPM in the absence of inhibitor. In this model, R_s is the solution resistance, R_{layer} the fluid resistance through the porous $FeCO_3$ corrosion layer, R_{ct} is the charge transfer resistance, while CPE_{layer} and CPE_{dl} are constant phase elements associated with the capacitance of the layer formed by the corrosion products and double electrochemical impedance, respectively. The CPE is used due to the dispersion effect caused by the heterogeneities at the metal surface such as roughness. The inductive loop observed at low frequency is fitted by R_L (inductive resistance) and L (inductance), which are associated with a adsorption/desorption controlled process of intermediate species and oil phase [16, 53]. On the other hand, the equivalent circuit in Figure 7B represents the sample evaluated at 1000 RPM in the absence of inhibitor, where R_w and Z_w are the Warburg impedance resistance and module associated with species diffusion through the corrosion product layer. The other elements of the equivalent circuit are the same than those presented in Figure 7A. Therefore, the results suggest that, at 1000 RPM, the experimental conditions promoted the formation of a denser $FeCO_3$ layer. In fact, this result supports the EIS results presented previously in this work where both charge and mass transfer processes were

identified for the sample evaluated at 1000 RPM. In this sample, the good performance obtained can be then attributed to a more compact corrosion product layer formed on the steel surface when compared to the rest of conditions, making the diffusion process in the corrosion product layer the rate determining step of both anodic and cathodic reactions [54].

Table 5 presents a summary of the equivalent circuit parameters obtained after fitting the EIS data for the samples evaluated in the absence of inhibitor. Interestingly, those evaluated at the lowest rotational speeds displayed the highest n_{layer} and n_{dl}. The "*n*" values are associated with the surface roughness due to corrosion effects. Where an "*n*" value close to 1 is related to low surface roughness promoted by low corrosion rates. Conversely, "*n*" values close to 0.5 are associated with high roughness due to high dissolution rates [55]. As a result, the increment in the "n_{dl}" value observed for the sample evaluated at 1000 RPM can be associated with the presence of a corrosion product layer on the steel surface, which, as explained above, was likely denser and more compact as compared with those in the other samples.

Figure 7C, D, and E shows the equivalent circuits models obtained after fitting the EIS data of the samples evaluated in the presence of inhibitor. A summary of the equivalent circuit parameters is also presented in Table 6. The results show the highest R_{ct} and R_{film} values in the samples evaluated at the lowest rotational speeds (10 and 100 RPM), where R_{film} and CPE_{film} are the resistance and capacitance of the inhibitor film, respectively. This model can be associated with the formation of a protective film of inhibitor on the metal surface [55], which is consistent with the n_{film} and n_{dl} values close to 1 found for these conditions. However, when the rotational speed was increased at 500 and 2000 RPM, the equivalent model changes as observed in Figure 7D, adding the R_L and L parameters to the model. This change is associated with the desorption of the inhibitor on the metal surface. This behavior is also consistent with the n_{film}, $n_{ct,}$ R_{film}, and R_{ct} values obtained, indicating a higher dissolution rate with respect to the samples evaluated at 10 and 100 RPM. On the other hand, the sample evaluated at 1000 RPM had a different equivalent circuit as shown in Figure 7E. This model is related to the amount of inhibitor adsorbed on the metal surface. For instance, the turbulent flow influences the electrode wall shear stress and can promote an inhibitor absorption/desorption process. Z_w is the Warburg impedance associated with a diffusion process, such as ions passing through the pores within the corrosion product layer [56]. Overall, although the turbulent flow seems to reduce the corrosion resistance of the steel surface, it can be observed from the results in Tables 5 and 6 that, for practical applications, the corrosion protection is still better in the presence of the inhibitor. In this sense, the use of an inhibitor to protect the steel surface under flow conditions and also, if possible, a decrease in the fluid movement are advisable strategies to maximize the inhibitor action on the metal surface.

Table 5. Equivalent circuit parameters obtained after fitting the EIS data in the absence of inhibitor.

Rotational speed (RPM)	R_s (Ω·cm²)	R_{layer} (Ω·cm²)	CPE_{layer} (F/cm²)	n_{layer}	R_{ct} (Ω˙cm²)	CPE_{ct} (F/cm²)	n_{dl}	R_L (Ω·cm²)	L (H·cm⁻²)	R_w (Ω·cm²)	Z_W
10	233.7	263	8.82×10^{-5}	0.792	978	2.3×10^{-4}	0.9	948.5	99.22		
100	39.05	227.2	2.62×10^{-4}	0.897	345	9.2×10^{-2}	0.999	129.2	11698		
500	11.23	56.56	8.19×10^{-4}	0.869	102	5.7×10^{-2}	0.634	157.1	989.5		
1000	82	73.71	6.18×10^{-5}	0.360	2928	1.03×10^{-4}	0.826			2701	14921
2000	61.18	140.8	3.09×10^{-3}	0.589	310	7.9×10^{-2}	0.6	200.9	436.9		

Table 6. Equivalent circuit parameters obtained after fitting the EIS data in the presence of inhibitor.

Rotational speed (RPM)	R_s (Ω·cm²)	R_{film} (Ω·cm²)	CPE_{film} (F/cm²)	n_{film}	R_{ct} (Ω·cm²)	CPE_{ct} (F/cm²)	n_{dl}	R_L (Ω˙cm²)	L (H·cm⁻²)	R_w (Ω˙cm²)
10	739.7	1975	4.04×10^{-5}	0.711	14788	2.46×10^{-5}	0.935			
100	1734	1473	2.04×10^{-5}	0.792	53178	2.78×10^{-5}	0.858			
500	46.28	610.7	8.56×10^{-5}	0.487	6656	8.20×10^{-5}	0.584	3599	4228	
1000	57.09	339.1	9.59×10^{-6}	0.805	7082	1.92×10^{-4}	0.482			6.69
2000	28.42	78.64	6.12×10^{-5}	0.710	300	6.04×10^{-4}	0.600	405.5	25.47	

3.4. SEM analysis

Sample rotational speeds	Inhibitor-free solution	Inhibited solution
0 RPM	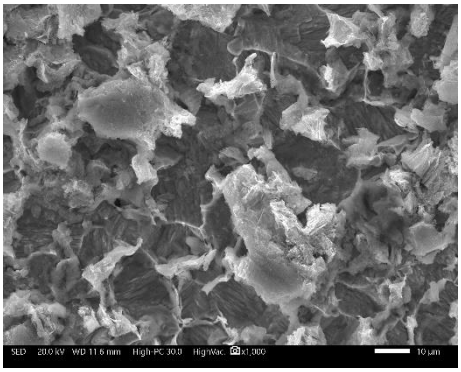	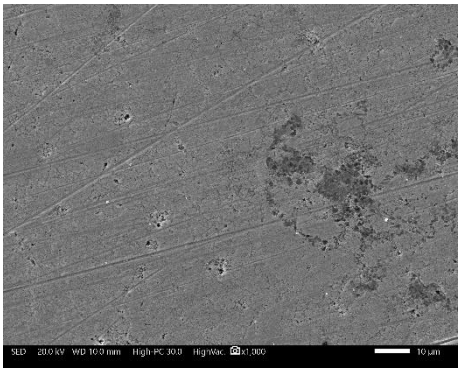
10 RPM	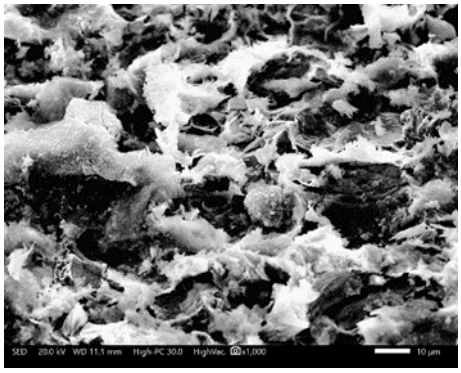	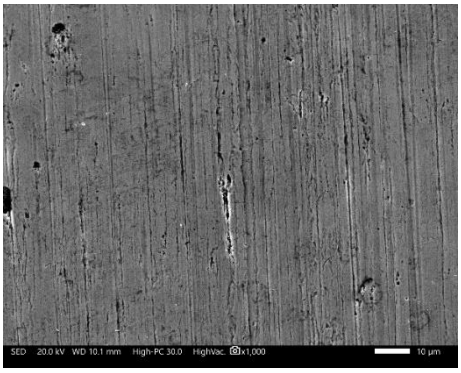
100 RPM	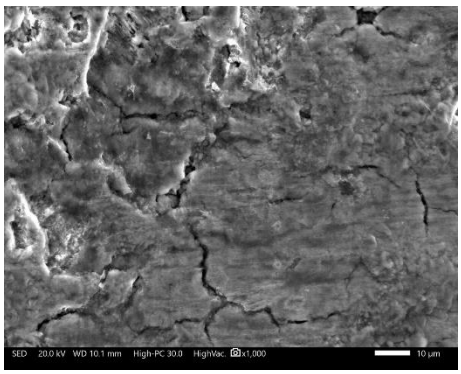	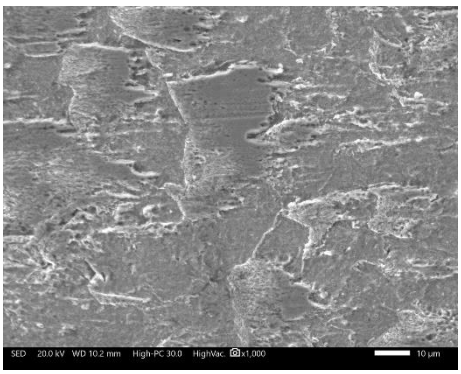
500 RPM	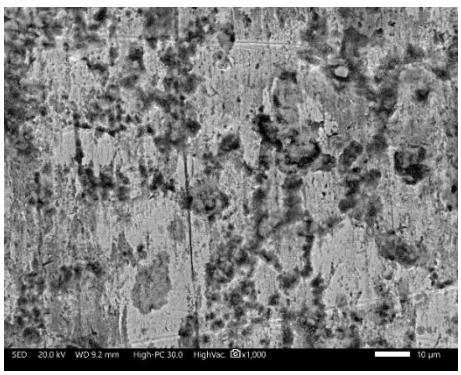	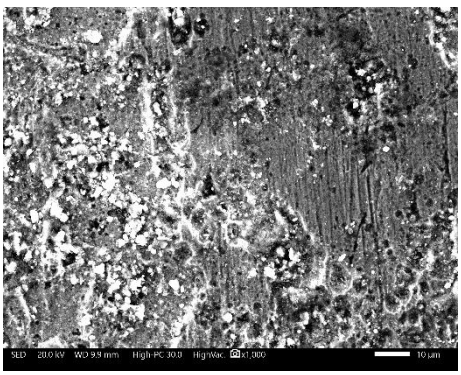

Sample rotational speeds	Inhibitor-free solution	Inhibited solution
1000 RPM	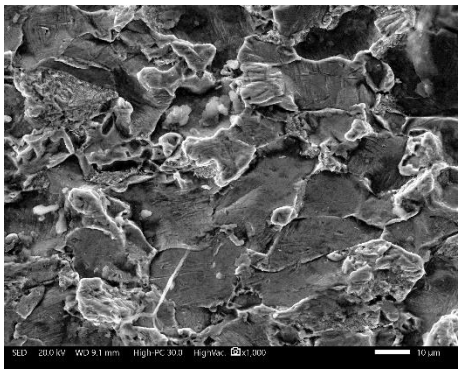	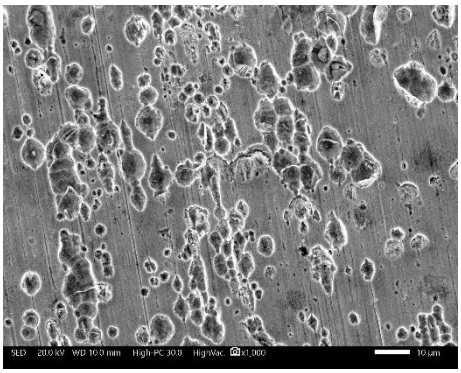
2000 RPM	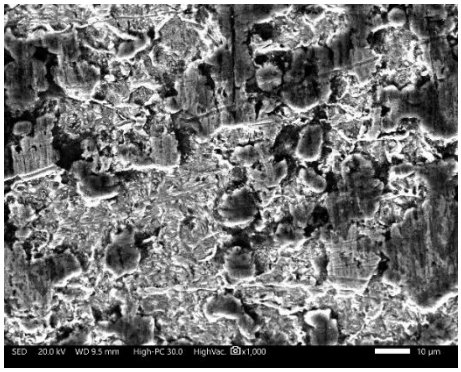	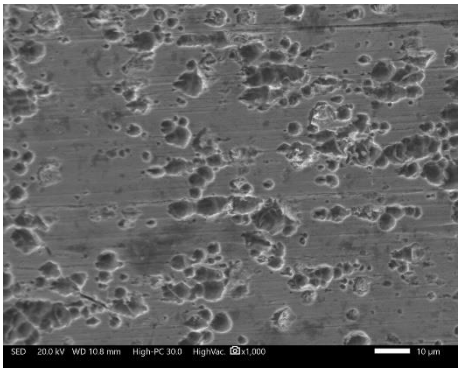

Figure 8. SEM analysis of the 1080 carbon steel samples evaluated in the presence and absence of inhibitor in a 3%NaCl–diesel solution with bubbling CO_2 at different rotational speeds.

Figure 8 shows the SEM micrograph of the steel samples evaluated in the absence and presence of inhibitor. The results in the absence of inhibitor and under static conditions (0 RPM) show the formation of a corrosion product layer ($FeCO_3$ layer), which had a poor protective role against corrosion, displaying the worse corrosion resistance among the samples studied in this work. The formation of the $FeCO_3$ layer was also observed for all the samples evaluated in the absence of inhibitor. However, this layer presented different characteristics as a function of the rotational speed. For example, at 10 RPM, the $FeCO_3$ layer had a similar morphology than that observed at 0 RPM. At 100 RPM, the corrosion layer displays some cracks, whereas at 500 and 1000 RPM, the corrosion layer seems to growth mostly porous and dense, respectively. In addition, at 2000 RPM, the results show the formation of large pits in the $FeCO_3$ layer, which were likely formed due to the partial dissolution of the latter during the test. The initiation and propagation of localized corrosion on the carbon steel surface under sweet corrosion is often conducted firstly by a local breakdown of the protective layer and development of a galvanic cell. In this case, the chloride ions could cause pitting corrosion and could readily attack the steel surface by

modifying the ionic strength of solution at the steel–solution interface by promoting the formation of soluble iron chloride complex species. Thus, soluble iron chloride complex compounds can lead to the delamination of the corrosion products due to the momentum provided by the rotating electrode, especially under turbulent flow conditions [57]. Schmit *et al.* reported that, under subcritical flow intensities, a mechanism of pitting can initiate a flow induced localized corrosion (FILC), which is firstly associated with an increase in the cracking tendency of the $FeCO_3$ layer, followed by spalling and the initiation of FILC [13]. Interestingly, the SEM analysis support the results obtained in the electrochemical testing of the steel samples in the absence of inhibitor. In particular, the samples with the poorest electrochemical performance were those showing a corrosion product layer with the presence of porosity, cracks, or pitting. The sample with the best protective behavior was that evaluated at 1000 RPM, which displayed a dense protective layer.

On the other hand, in the presence of inhibitor, at 0 and 10 RPM, the samples showed a rough pattern induced during the metallographic preparation process. This roughness was visible before immersion of the samples in the electrolyte; this observation suggests an inhibited corrosion process. In fact, when the rotating rate was increased, the corrosion rate also increased, in particular above 100 RPM. The sample evaluated at 100 RPM shows the formation of a $FeCO_3$ layer. However, at 500 RPM, the samples presented pitting on the surface of the $FeCO_3$ scales. Analyzing samples evaluated at 1000 and 2000 RPM, a severe localized corrosion process can be observed, which resulted in the formation of pits. This fact was likely promoted by the presence of scratches produced from the metallographic preparation, causing the pits to be aligned in the same orientation of such scratches [57]. This phenomenon agrees with the electrochemical results presented in this work that associate the movement of the fluid to the concentration of inhibitor adsorbed at the metal surface. Under rotation some places on the metal surface remain uncovered by the inhibitor, behaving as active sites where localized corrosion process can take place [24]. Therefore, this result confirms that the inhibitor concentration is important to avoid corrosion, in this case, localized corrosion. In addition, the fluid movement is a key factor that influences the concentration of inhibitor at the metal surface, when the fluid movement is too large, the inhibitor efficiency decreases drastically [58].

Figures 9–13 show a schematic representation of the models used to support the phenomena mentioned in this work. Figures 9 and 10 describe the corrosion behavior of the 1018 carbon steel alloy in absence of inhibitor, displaying, for all rotating rates, a $FeCO_3$ porous layer. Under these conditions, the adsorption of a thin film of diesel is promoted. The pore size, precipitation and formation of the $FeCO_3$ layer, and diesel adsorption, are a function of the rotating rate. The results show a $FeCO_3$ layer denser at 1000 RPM with respect to the other rotating rates (see Figures 8 and 10) and, coupled with the diesel adsorption, this rotation rate led to an increase in the corrosion resistance.

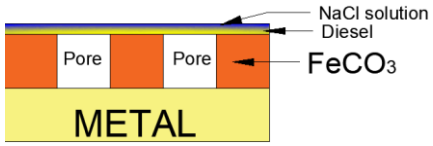

Figure 9. Model used to describe the behavior of the carbon steel alloy in NaCl–CO_2 solution without inhibitor at 0, 10, 100, 500 and 2000 RPM.

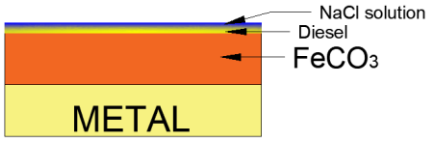

Figure 10. Model used to describe the behavior of the carbon steel alloy in NaCl–CO_2 without inhibitor at 1000 RPM.

On the other hand, Figures 11, 12 and 13 show the schematic representation of the models that describe the corrosion behavior according to the results using the inhibitor in this work. Figure 11 describes the inhibitor adsorption during the first's hours of test for all the rotating rates. Figure 12 shows the stabilization of the inhibitor molecules on the surface, which provides protection to the metal surface. From 500 to 2000 RPM, the highest rotation rate can lead to inhibitor desorption and permeation of water molecules through the pores, reducing the corrosion resistance.

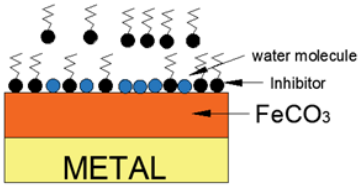

Figure 11. Model used to describe the behavior of the carbon steel alloy in NaCl–CO_2 solution with inhibitor during the first´s hours of test (adsorption).

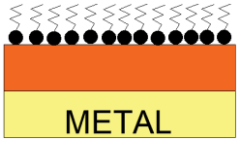

Figure 12. Model used to describe the behavior of the carbon steel alloy in NaCl–CO_2 solution with inhibitor at 0, 10 and 100 RPM (inhibitor establishing).

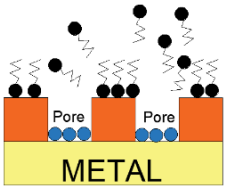

Figure 13. Model used to describe the behavior of the carbon steel alloy in NaCl–CO_2 solution with inhibitor at 500, 1000 and 2000 RPM (desorption).

4. Conclusions

The corrosion resistance of a commercial 1018 carbon steel was studied in the absence and presence of a green corrosion inhibitor under hydrodynamic flow conditions. In the absence of inhibitor, the highest corrosion resistances were reached for a rotational speed value of 1000 RPM, which is attributed to the precipitation of a protective $FeCO_3$ layer resulting in turn from a mass transport competing process of $HCO_3^-$and H^+ and adsorption of oil species at the metal surface. Hydrodynamic flow conditions promote the formation of a $FeCO_3$ layer as a function of the rotational speed, which presents the best performance when the formed layer becomes denser. Thus, the use of fluid movement for uninhibited carbon steel surfaces is recommended in order to increase the corrosion resistance of the surface, especially employing fluid movement that can improve the formation of the protective $FeCO_3$ layer.

In the presence of inhibitor, the best corrosion resistance was obtained under static flow conditions. The increment in the rotational speed showed a remarkable increase in the corrosion rate, in particular when the rotational speed was increased beyond 100 RPM. This behavior is associated with the negative hydro-mechanical effect on the metal surface that tends to change the inhibitor concentration at the surface due to the significant wall shear stress produced by the fluid. This fact results in some unprotected metal areas in contact with the corrosive medium, making them active sites where a localized corrosion process can take place. Hydrodynamic flow conditions are not recommended when an inhibitor is used for corrosion protection of steels; however, if the fluid movement is a must, then it should be as low as possible to avoid a drastic desorption of the inhibitor film at the metal surface. Anywise, the use of an inhibitor is better for corrosion protection even under hydrodynamic flow conditions, bearing in mind that the inhibitor performance decreases with the fluid movement.

Acknowledgment

O. Sotelo-Mazon is thankful to the postdoctoral fellowship DGAPA-UNAM. Dr. John Henao also acknowledges to the CONACYT program “Investigadores por México” – project 848 for the support during the development of this work.

References

1. M.W. Faraj and A. Alamiery, Palm oil as green corrosion inhibitors for different metal surfaces and corrosive media: A review, *Int. J. Corros. Scale Inhib*., 2022, **11**, no. 2, 465–477. doi: 10.17675/2305-6894-2022-11-2-1
2. Y. Ma, Y. Li and F. Wang, Corrosion of low carbon steel in atmospheric environments of different chloride content, *Corros. Sci*., 2009, **51**, no. 5, 997–1006. doi: https://doi.org/10.1016/j.corsci.2009.02.009
3. M.B. Kermani and A. Morshed, Carbon Dioxide Corrosion in Oil and Gas Production – A Compendium, *Corrosion*, 2003, **59**, no. 8, 659–683. doi: 10.5006/1.3277596

4. R.A. De Motte, R. Barker, D. Burkle, S.M. Vargas and A. Neville, The Early Stages of $FeCO_3$ Scale Formation Kinetics in CO_2 Corrosion, *Mater. Chem. Phys*., 2018, **216**, 102–111. doi: 10.1016/j.matchemphys.2018.04.077
5. G. Zhang, C. Chen, M. Lu, C. Chai and Y. Wu, Evaluation of inhibition efficiency of an imidazoline derivative in CO_2-containing aqueous solution, *Mater. Chem. Phys*., 2007, **105**, no. 2–3, 331–340. doi: 10.1016/j.matchemphys.2007.04.076
6. B.J. Usman and S.A. Ali, Carbon dioxide corrosion inhibitors: A review, *Arab. J. Sci. Eng*., 2017, **43**, no. 1, 1–22. doi: 10.1007/s13369-017-2949-5
7. L.M. Rivera-Grau, M. Casales, I. Regla, D.M. Ortega-Toledo, J.G. Gonzalez-Rodriguez and L. Martinez Gomez, CO_2 Corrosion inhibition by imidazoline derivatives based on coconut oil, *Int. J. Electrochem. Sci*., 2012, **7**, 13044–13057. Link
8. I.A. Aiad, A.A. Hafiz, M.Y. El-Awady and A.O. Habid, Some imidazoline derivatives as corrosion inhibitors, *J. Surfact. Deterg*., 2010, **13**, 247–254. doi: 10.1007/s11743-009-1168-9
9. M.E. Olvera-Martinez, J. Mendoza-Flores and J. Genesca, CO_2 corrosion control in steel pipelines. Influence of turbulent flow on the performance of corrosion inhibitors, *J. Loss Prev. Process Ind*., 2015, **35**, 19–28. doi: 10.1016/j.jlp.2015.03.006
10. O. Sotelo-Mazon, S. Valdez-Rodriguez, J. Porcayo-Calderon, M. Casales-Díaz, J. Henao, G. Salinas-Solano, J.L. Valenzuela-Lagarda and L. Martinez-Gomez, Corrosion protection of 1018 carbon steel using an avocado oil-based inhibitor, *Green Chem. Lett. Rev*., 2019, **12**, no. 3, 255–270. doi: 10.1080/17518253.2019.1629698
11. Y. Seung-Hyun, K. Young-Wun, C. Kunwoo, B. Seung-Yeop and K. Joon-Seop, Synthesis and corrosion inhibition behavior of imidazoline derivatives based on vegetable oil, *Corros. Sci*., 2012, **59**, 42–54. doi: 10.1016/j.corsci.2012.02.011
12. D.C. Silverman, Rotating cylinder electrode for velocity sensitivity testing, *Corrosion*, 1984, **40**, no. 5, 220–226. doi: 10.5006/1.3581945
13. G.A. Schmitt and M. Mueller, Critical wall shear stresses in CO_2 corrosion of carbon steel, *NACE Corrosion*, 1999, **44**, NACE-99044. Link
14. S. Nešić, G.T. Solvi and S. Skjerve, Comparison of rotating cylinder and loop methods for testing CO_2 corrosion inhibitors, *Br. Corros. J*., 1997, **32**, no. 4, 269–276. doi: 10.1179/000705997798129188
15. *I Low-carbon, Classification and Designation of Carbon and Low-Alloy Steels, ASM Handbooks Vol. 1*, Properties and Selection: Irons, Steels, and High-Performance Alloys, ASM International, 2005.
16. O. Sotelo-Mazon, S. Valdez, J. Porcayo-Calderon, J. Henao, C. Cuevas-Arteaga, C.A. Poblano-Salas and L. Martinez-Gomez, Evaluation of corrosion inhibition of 1018 carbon steel using an avocado oil-based green corrosion inhibitor, *Prot. Met. Phys. Chem*., 2020, **56**, 427–437. doi: 10.1134/S2070205120020240

17. J.L. Mora-Mendoza, J.G. Chacon-Nava, G. Zavala-Olivares, M.A. González-Núñez and S. Turgoose, Influence of turbulent flow on the localized corrosion process of mild steel with inhibited aqueous carbon dioxide systems, *Corrosion*, 2002, **58**, no. 7, 608–619. doi: 10.5006/1.3277652
18. W. Li, Y. Xiong, B. Brown, K.E. Kee and S. Nešić, Measurement of wall shear stress in multiphase flow and its effect on protective $FeCO_3$ corrosion product layer removal, *NACE Corrosion*, 2015, 5922, NACE-2015-5922. Link
19. D.C. Silverman, The rotating cylinder electrode for examining velocity-sensitive corrosion – A review, *Corrosion*, 2004, **60**, no. 11, 1003–1023. doi: 10.5006/1.3299215
20. S. Ghareba and S. Omanovic, The effect of electrolyte flow on the performance of 12-aminododecanoic acid as a carbon steel corrosion inhibitor in CO_2-saturated hydrochloric acid, *Corros. Sci*., 2011, **53**, no. 11, 3812–3805. doi: 10.1016/j.corsci.2011.07.031
21. I.B. Onyeachu, I.B. Obot, A.A. Sorour and M.I. Abdul-Rashid, Green corrosion inhibitor for oilfield application I: Electrochemical assessment of 2-(2-pyridyl) benzimidazole for API X60 steel under sweet environment in NACE brine ID196, *Corros. Sci*., 2019, **150**, 183–193. doi: 10.1016/j.corsci.2019.02.010
22. A.Y. Musa, A.A.H. Kadhum, A.B. Mohamad, A.R. Daud, M.S. Takriff, S.K. Kamarudin and N. Muhamad, Stability of layer forming for corrosion inhibitor on mild steel surface under hydrodynamic conditions, *Int. J. Electrochem. Sci*., 2009, **4**, 707–716. Link
23. I.B. Onyeachu, D.S. Chauhan, M.A. Quraishi and I.B. Obot, Influence of hydrodynamic condition on 1,3,5-tris(4-methoxyphenyl)-1,3,5-triazinane as a novel corrosion inhibitor formulation for oil and gas industry, *Corros. Eng. Sci. Technol*., 2020, **56**, no. 2, 154–161. doi: 10.1080/1478422X.2020.1827348
24. D.M. Ortega-Toledo, J.G. Gonzalez-Rodriguez, M. Casales, L. Martinez and A. Martinez-Villafañe, CO_2 corrosion inhibition of X-120 pipeline steel by a modified imidazoline under flow conditions, *Corros. Sci*., 2011, **53**, no. 11, 3780–3787. doi: 10.1016/j.corsci.2011.07.028
25. F.F. Eliyan, F. Mohammadi and A. Alfantazi, An electrochemical investigation on the effect of the chloride content on CO_2 corrosion of API-X100 steel, *Corros. Sci*., 2012, **64**, 37–43. doi: 10.1016/j.corsci.2012.06.032
26. E. Rodriguez-Clemente, J.G. Gonzalez-Rodriguez, M.G. Valladares-Cisneros and J.G. Chacon-Nava. Evaluation of allium sativum as corrosion inhibitor for carbon steel in sulphuric acid under hydrodynamic conditions, *Green Chem. Lett. Rev*., 2015, **8**, no. 2, 49–58. doi: 10.1080/17518253.2015.1071435
27. N. Ochoa, F. Moran, N. Pébère and B. Tribollet, Influence of flow on the corrosion inhibition of carbon steel by fatty amines in association with phosphonocarboxylic acid salts, *Corros. Sci*., 2005, **47**, no. 3, 604–593. doi: 10.1016/j.corsci.2004.07.021

28. A. Cruz-Zabalegui, E. Vazquez-Velez, G. Galicia-Aguilar, M. Casales-Diaz, R. Lopez-Sesenes, J.G. Gonzalez-Rodriguez and L. Martinez-Gomez, Use of a non-ionic gemini-surfactant synthesized from the wasted avocado oil as a CO_2- corrosion inhibitor for X-52 steel, *Ind. Crops Prod*., 2019, **133**, 203–211. doi: 10.1016/j.indcrop.2019.03.011
29. A. Cáceres, M. Casales and L. Martínez, A comparative study of gravimetric and electrochemical techniques for the evaluation of corrosion inhibitor activity onset and efficiency in pipeline CO_2 environments, *Rev. Chil. Ing*., 2019, **27**, no. 4, 625–634. Link
30. J. Porcayo-Calderon, M. Casales-Diaz, L.M. Rivera-Grau, D.M. Ortega-Toledo, J.A. Ascencio-Gutierrez and L. Martinez-Gomez, Effect of the diesel, inhibitor, and CO_2 additions on the corrosion performance of 1018 carbon steel in 3% NaCl solution, *J. Chem*., **2014**, 2014, 1–10. doi: 10.1155/2014/940579
31. H. Zhang, K. Gao, L. Yan and X. Pang, Inhibition of the corrosion of X70 and Q235 steel in CO_2-saturated brine by imidazoline-based inhibitor, *J. Electroanal. Chem*., 2017, **791**, 83–94. doi: 10.1016/j.jelechem.2017.02.046
32. J. Han, D. Young, H. Colijn, A. Tripathi and S. Nešić, Chemistry and structure of the passive film on mild steel in CO_2 corrosion environments, *Ind. Eng. Chem. Res*., 2009, **48**, no. 13, 6296–6302. doi: 10.1021/ie801819y
33. N. Srisuwan, N. Ochoa, N. Pébère and B. Tribollet, Variation of carbon steel corrosion rate with flow conditions in the presence of an inhibitive formulation, *Corros. Sci*., 2008, **50**, no. 5, 1245–1250. doi: 10.1016/j.corsci.2008.01.029
34. Y. Hua, R. Barker and A. Neville, Comparison of corrosion behaviour for X-65 carbon steel in supercritical CO_2-saturated water and water-saturated/unsaturated supercritical CO_2, *J. Supercrit. Fluids*, 2015, **97**, 224–237. doi: 10.1016/j.supflu.2014.12.005
35. Y. Hua, S. Xu, Y. Wang, W. Taleb, J. Sun, L. Zhang, R. Barker and A. Neville, The formation of $FeCO_3$ and Fe_3O_4 on carbon steel and their protective capabilities against CO_2 corrosion at elevated temperature and pressure, *Corros. Sci*., 2019, **157**, 392–405. doi: 10.1016/j.corsci.2019.06.016
36. J. Porcayo-Calderon, I. Regla, E. Vazquez-Velez, L.M. Martinez de la Escalera, J. Canto and M. Casales-Diaz, Effect of the Unsaturation of the Hydrocarbon Chain of Fatty-Amides on the CO_2 Corrosion of Carbon Steel Using EIS and Real-Time Corrosion Measurement, *J. Spectro*., 2015, **2015**, 1–13. doi: 10.1155/2015/184140
37. R. Galvan-Martinez, R. Orozco-Cruz, R. Torres-Sanchez and E.A. Martinez, Corrosion study of the X52 steel immersed in seawater with a corrosion inhibitor using a rotating cylinder electrode, *Mater. Corros*., 2010, **61**, no. 10, 872–876. doi: 10.1002/maco.200905441
38. W. Villamizar, M. Casales, J.G. Gonzalez-Rodriguez and L. Martinez, CO_2 corrosion inhibition by hydroxyethyl, aminoethyl, and amidoethyl imidazolines in water–oil mixtures, *J. Solid State Electrochem*., 2007, **11**, 619–629. doi: 10.1007/s10008-006-0208-x

39. E. Gulbrandsen, S. Nešić, A. Stangeland and T. Burchardtt, Effect of precorrosion on the performance of inhibitor for CO_2 corrosion of carbon steel, *NACE Corrosion*, 1998, **13**, NACE-98013. Link
40. E. Barmatov and T.L. Hughes, Effect of corrosion products and turbulent flow on inhibition efficiency of propargyl alcohol on AISI 1018 mild carbon steel in 4 M hydrochloric acid, *Corros. Sci*., 2017, **123**, 170–181. doi: 10.1016/j.corsci.2017.04.020
41. H. Ashassi-Sorkhabi and E. Asghari, Effect of hydrodynamic conditions on the inhibition performance of l-methionine as a "green" inhibitor, *Electrochim. Acta*, 2008, **54**, no. 2, 162–167. doi: 10.1016/j.electacta.2008.08.024
42. X. Jiang, Y.G. Zheng and W. Ke, Effect of flow velocity and entrained sand on inhibition performances of two inhibitors for CO_2 corrosion of N80 steel in 3% NaCl solution, *Corros. Sci*., 2005, **47**, no. 11, 2636–2658. doi: 10.1016/j.corsci.2004.11.012
43. H.H. Hassan, Inhibition of mild steel corrosion in hydrochloric acid solution by triazole derivatives Part II: Time and temperature effects and thermodynamic treatments, *Electrochim. Acta*, 2007, **53**, no. 4, 1722–1730. doi: 10.1016/j.electacta.2007.08.021
44. J.B. Sun, G.A. Zhang, W. Liu and M.X. Lu, The formation mechanism of corrosion scale and electrochemical characteristic of low alloy steel in carbon dioxide-saturated solution, *Corros. Sci*., 2012, **57**, 131–138. doi: 10.1016/j.corsci.2011.12.025
45. Z.F. Yin, Y.R. Feng, W.Z. Zhao, Z.Q. Bai and G.F. Lin, Effect of temperature on CO_2 corrosion of carbon steel, *Surf. Interface Anal*., 2009, **41**, 517–523. doi: 10.1002/sia.3057
46. S. Nešić, G.T. Solvi and J. Enerhaug, Comparison of the Rotating Cylinder and Pipe Flow Tests for Flow-Sensitive Carbon Dioxide Corrosion, *Corrosion*, 1995, **51**, no. 10, 773–787. doi: 10.5006/1.3293555
47. D.A. Lopez, S.N. Simison and S.R. de Sanchez, Inhibitors performance in CO_2 corrosion EIS studies on the interaction between their molecular structure and steel microstructure, *Corros. Sci*., 2005, **47**, no. 3, 735–755. doi: 10.1016/j.corsci.2004.07.010
48. D.A. Lopez, S.N. Simison and S.R. de Sanchez, The influence of steel microstructure on CO_2 corrosion. EIS studies on the inhibition efficiency of benzimidazole, *Electrochim. Acta*., 2003, **48**, no. 7, 845–854. doi: 10.1016/S0013-4686(02)00776-4
49. K. Alawadhi, A.S. Aloraier, S. Joshi, J. Alsarraf and S. Swilem, Investigation on preferential corrosion of welded carbon steel under flowing conditions by EIS, *J. Mater. Eng. Perform*., 2013, **22**, no. 8, 2403–2410. doi: 10.1007/s11665-013-0525-z
50. A. Popova, S. Raicheva, E. Sokolova and M. Christov, Frequency dispersion of the interfacial impedance at mild steel corrosion in acid media in the presence of benzimidazole derivatives, *Langmuir*, 1996, **12**, no. 8, 2083–2089. doi: 10.1021/la950148+

51. A. Shamsa, R. Barker, Y. Hua, E. Barmatov, T.L. Hughes and A. Neville, Impact of corrosion products on performance of imidazoline corrosion inhibitor on X65 carbon steel in CO_2 environments, *Corros. Sci*., 2021, **185**, 1–16. doi: 10.1016/j.corsci.2021.109423
52. Y.J. Tan, S. Bailey and B. Kinsella, An investigation of the formation and destruction of corrosion inhibitor films using electrochemical impedance spectroscopy (EIS), *Corros. Sci*., 1996, **38**, no. 9, 1545–1561. doi: 10.1016/0010-938X(96)00047-9
53. Ln. Xu, Jy. Zhu, Mx. Lu, L. Zhang and W. Chang, Electrochemical impedance spectroscopy study on the corrosion of the weld zone of 3Cr steel welded joints in CO_2 environments, *Int. J. Miner. Metall. Mater*., 2015, **22**, no. 5, 500–508. doi: 10.1007/s12613-015-1099-6
54. Gx. Zhao, Xh. Lu, Jm. Xiang and Y. Han, Formation characteristic of CO_2 corrosion product layer of P110 steel investigated by SEM and electrochemical techniques, *J. Iron Steel Res. Int*., 2009, **16**, no. 4, 89–94. doi: 10.1016/S1006-706X(09)60067-4
55. N.B. Gomez-Guzman, J. Porcayo-Calderon and J.G. Gonzalez-Rodriguez, Corrosion inhibition of X70 pipeline steel under hydrodynamic conditions of CO_2 with amide extraction from coffee bagasse, *J. Bio. Tribo. Corros*., 2021, **7**, no. 86, 1–15. doi: 10.1007/s40735-021-00523-6
56. Y. Chen, T. Hong, M. Gopal and W.P. Jepson, EIS studies of a corrosion inhibitor behavior under multiphase flow conditions, *Corros. Sci*., 2000, **42**, no. 6, 979–990. doi: 10.1016/S0010-938X(99)00127-4
57. I.B. Obot, I.B. Onyeachu and S.A. Umoren, Alternative corrosion inhibitor formulation for carbon steel in CO_2-saturated brine solution under high turbulent flow condition for use in oil and gas transportation pipelines, *Corros. Sci*., 2019, **159**, 1–19. doi: 10.1016/j.corsci.2019.108140
58. Hh. Zhang, X. Pang and K. Gao, Localized CO_2 corrosion of carbon steel with different microstructures in brine solutions with an imidazoline-based inhibitor, *Appl. Surf. Sci*., 2018, **442**, no. 1, 446–460. doi: 10.1016/j.apsusc.2018.02.115

♦ ♦ ♦